Petroleum Science 21 (2024) 1751–1764

Contents lists available at ScienceDirect

Petroleum Science

journal homepage: www.keaipublishing.com/en/journals/petroleum-science

Original Paper

Inter-layer interference for multi-layered tight gas reservoir in the absence and presence of movable water

Tao Zhang [a, *], Bin-Rui Wang [a], Yu-Long Zhao [a], Lie-Hui Zhang [a], Xiang-Yang Qiao [b], Lei Zhang [b], Jing-Jing Guo [a], Hung Vo Thanh [c]

[a] National Key Laboratory of Oil and Gas Reservoir Geology and Exploitation, Southwest Petroleum University, Chengdu, 610500, Sichuan, China
[b] Shaanxi Yanchang Petroleum (Group) Corp. Ltd., Xi'an, 710075, Shaanxi, China
[c] Waseda Research Institute for Science and Engineering, Waseda University, Tokyo, Japan

ARTICLE INFO

Article history:
Received 14 October 2023
Received in revised form
5 January 2024
Accepted 10 January 2024
Available online 11 January 2024

Edited by Yan-Hua Sun

Keywords:
Tight gas
Comingled production
Interference
Two-phase flow
Water blocking

ABSTRACT

Due to the dissimilarity among different producing layers, the influences of inter-layer interference on the production performance of a multi-layer gas reservoir are possible. However, systematic studies of inter-layer interference for tight gas reservoirs are really limited, especially for those reservoirs in the presence of water. In this work, five types of possible inter-layer interferences, including both absence and presence of water, are identified for commingled production of tight gas reservoirs. Subsequently, a series of reservoir-scale and pore-scale numerical simulations are conducted to quantify the degree of influence of each type of interference. Consistent field evidence from the Yan'an tight gas reservoir (Ordos Basin, China) is found to support the simulation results. Additionally, suggestions are proposed to mitigate the potential inter-layer interferences. The results indicate that, in the absence of water, commingled production is favorable in two situations: when there is a difference in physical properties and when there is a difference in the pressure system of each layer. For reservoirs with a multi-pressure system, the backflow phenomenon, which significantly influences the production performance, only occurs under extreme conditions (such as very low production rates or well shut-in periods). When water is introduced into the multi-layer system, inter-layer interference becomes nearly inevitable. Perforating both the gas-rich layer and water-rich layer for commingled production is not desirable, as it can trigger water invasion from the water-rich layer into the gas-rich layer. The gas-rich layer might also be interfered with by water from the neighboring unperforated water-rich layer, where the water might break the barrier (eg weak joint surface, cement in fractures) between the two layers and migrate into the gas-rich layer. Additionally, the gas-rich layer could possibly be interfered with by water that accumulates at the bottom of the wellbore due to gravitational differentiation during shut-in operations.

1. Introduction

Natural gas, being a clean and highly economically efficient energy source, has accounted for nearly a quarter of global primary energy consumption in the past decade (IEA, 2017; BP, 2018). In China, the rapid increase in production of tight gas (characterized by porosity < 10% and permeability < 0.1 mD) with an estimated 12 trillion cubic meters (Tcm) of technically recoverable reserves, points to a promising future for unconventional gas resources (Yang et al., 2012; He et al., 2013; BGR, 2014; Zaini et al., 2019). Due to the thin sand thickness and poor permeability of these tight formations, the strategy of commingled production is commonly adopted to enhance economic production for tight gas reservoirs in China (He et al., 2013; Zaini et al., 2019; Jiang et al., 2023).

For the commingled production of multi-layer reservoirs, engineers and researchers should pay attention to the potential interferences caused by the interactions among each producing layer. Early investigations into multi-layer gas reservoirs were mostly centered around theoretical models for predicting well production or gas in place, often without considering well interference. Lefkovits et al. (1961) were among the first to explore the transient process of multi-layer production. They concluded that the

* Corresponding author.
E-mail address: tobiascheuing@163.com (T. Zhang).

https://doi.org/10.1016/j.petsci.2024.01.009

production of each layer depends on the product of the layer permeability and thickness. Under the boundary-dominated flow pattern, El-Banbi and Wattenbarger (1996) proposed a model for predicting the production of each layer using material balance and stabilized gas flow equations. Additionally, they introduced a production prediction model for multi-layer reservoirs that considers non-Darcy flow and variable bottom-hole pressure (El-Banbi and Wattenbarger, 1997). Kuppe et al. (2000) employed changing bottom-hole pressure to calculate gas in place for multi-layer reservoirs, assuming no crossflow. Cox et al. (2003) evaluated multi-layer production performance during both the early transient stage and the later boundary-dominated stage, aiming to provide insights into ultimate recovery reserves. Rahman and Mattar (2007) presented an analytical solution to characterize transient flow for commingled production, especially when the production layers have unequal initial pressures.

Over the past decade, researchers have gradually come to acknowledge the influences of interlayer interference on the production performance of multi-layer gas reservoirs. Efforts spanning the theoretical, experimental, and simulation domains have been undertaken to uncover the dominant influencing factors and quantify interlayer interference during commingled production, particularly with the growing attention on unconventional reservoirs such as tight gas, shale gas, and coalbed methane. Juell and Whitson (2011) introduced a backpressure equation for multi-layer gas reservoirs, considering scenarios both with and without interlayer communication. Liu et al. (2012) defined a statistical function to examine the effects of various factors, including permeability differences, sand layer numbers, and perforation characteristics, on interlayer interference. Eisa et al. (2013) proposed an integrated workflow (involving multi-rate production logging data, multi-layer transient testing, nodal analysis, etc.) to assess the performance of multi-layer gas reservoirs in Bahrain. For multi-layer shale gas reservoirs, Milad et al. (2013) developed an iterative numerical simulation, assuming no formation crossflow, to couple wellbore and reservoir hydraulics for predicting pressure and production of individual layers. Wan and Yong (2015) conducted experimental investigations into the key influencing factors affecting deliverability and gas in place for multi-layer gas reservoirs, employing two parallel samples. Zhao et al. (Zhao and Wang, 2019a; Zhao et al., 2019b) utilized the lattice Boltzmann method (LBM) to quantify the effects of interlayer heterogeneity, permeability, and pressure contrast on the production performance of multi-layer coalbed methane reservoirs. Examining a case of a tight gas well in the eastern Ordos Basin (China), Wang et al. (2019) analyzed an instance of interlayer interference during concurrent production from three separate layers. Their findings suggested that gas or water backflow might occur in some layers, leading to a reduction in well productivity. Liu et al. (2020) employed three parallel tight sandstone samples in an experimental study to explore the relationship between flow rate and backflow time. They concluded that the shut-in operation is unfavorable for multi-layer commingled production. Zhong et al. (2022) constructed fuzzy comprehensive evaluation method to evaluate the contribution rate of the co-production layer for multilayer tight gas reservoir.

As seen above, the systematic study of inter-layer interference in tight gas reservoir is really limited, and the potential types of inter-layer interference have not been clearly identified. Unlike the tight gas reservoirs in North America, the main tight gas reservoirs in China are formed within continental or transitional geological settings, resulting in complex heterogeneity in terms of reservoir properties and the distribution of gas and water (Zhang et al., 2020; Yang et al., 2023). Consequently, rapid changes in gas and water distribution are commonly observed both vertically and horizontally within the target formations (Zhao et al., 2020, 2021). Moreover, tight reservoirs are characterized by small pores (leading to high capillary pressure), intricate pore structures, and elevated clay content (Qiao et al., 2020; Yin et al., 2020). Consequently, water is inherently present within the original formation, typically in higher quantities compared to conventional reservoirs (Bennion and Thomas, 2005). When water is introduced into the multi-layer system, it becomes essential to explore its potential impact on commingled production performances to ensure the efficient development of these reservoirs.

In this work, we propose five possible types of inter-layer interferences, encompassing both the presence and absence of water, for commingled production in tight gas reservoirs. Subsequently, based on the typical reservoir characteristics of the Yan'an tight gas reservoir in the Ordos Basin, China, we perform a series of numerical simulations at both reservoir-scale (using IMEX and CMG) and pore-scale (utilizing LBM) levels. These simulations aim to quantify the degree of influence exerted by each type of interference. To validate our findings, we utilize testing data (including well logging, fluid-producing profiles, pressure tests, etc.) as well as production data from tight gas wells within the Yan'an Gas Field. The field evidence we collected consistently supports the outcomes of our simulations. To the best of our knowledge, this work marks the first systematic investigation of inter-layer interference in commingled production of tight gas reservoirs.

2. Inter-layer interference

2.1. Possible patterns

2.1.1. Absence of water

During commingled production, inter-layer interference arises from the disparities among various producing layers. These disparities can be categorized as reservoir properties (such as porosity ϕ, permeability K, saturation S_w, layer thickness h, etc.) and environmental conditions (pressure p and temperature T). Among these factors, the parameters that notably influence the production performance of the multi-layer system can be condensed into the formation coefficient Kh and pressure p, as depicted in Fig. 1. During commingled production, the different layers are interconnected through the wellbore, allowing for the potential of dissimilarity-driven mass transfer between these layers. This interaction has the potential to lead to interference and subsequently reduce overall well production. Formation coefficient Kh is widely used to characterize the reservoir properties of each layer in multi-layer reservoirs, with layers possessing lower Kh values generally contributing less to production. Furthermore, due to the varying stages of gas migration and accumulation processes across geological time, the pressures between different layers are typically not uniform, particularly for those layers with significant vertical spans. Distinct pressure systems can result in different production contributions from each layer. Numerous investigations have been conducted to comprehend the inter-layer interference resulting from these two factors, yet a consensus has yet to be reached (Liu et al., 2020). It is important to note that, in this study, the term “gas-rich layer” (dry layer) signifies a layer with initial water

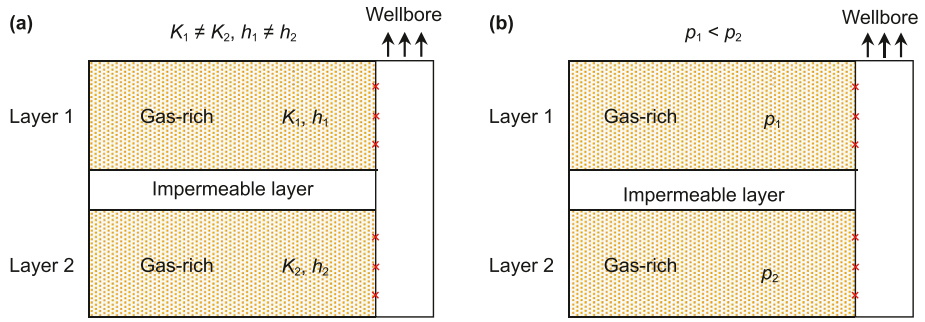

Fig. 1. Schematic diagram of inter-layer interference in absence of water (dry layer) due to difference in physical properties of the two layers (**a**), and multi-pressure system of the two layers (**b**). Red cross represents perforation; black arrow represents the flow direction of production fluid. *K* is permeability; *h* is the layer thickness; *P* is the layer pressure.

saturation below the irreducible water saturation.

2.1.2. Presence of water

As mentioned previously, formation water is widespread in tight gas reservoirs, and the complexities of inter-layer interference become much more pronounced in the presence of water. Nonetheless, the study of inter-layer interference under these circumstances remains limited. The intrusion of water shifts the flow from single-phase to gas/water two-phase flow. Gas flow pathways within the porous media are obstructed by the invading water, leading to a reduction in effective gas permeability. Furthermore, the intrusion of water induces migration or swelling of clay minerals, resulting in permanent damage to intrinsic permeability. In tight rock formations, the damage to effective gas permeability is even more severe due to the intricate structure and correspondingly higher likelihood of phase trapping (Shanley et al., 2004). The phenomenon known as the "relative permeability jail," where both water and gas relative permeabilities are very low over a range of saturations, might also occur (Shaoul et al., 2011). Consequently, when water is introduced into a previously dry production layer, substantial impairment to the layer deliverability is anticipated, leading to a subsequent decrease in well production.

The potential interference patterns can be categorized into three types (Fig. 2): (1) Interference due to unintentionally perforated water-rich layer: At the initial developmental stages of tight gas reservoirs, the unintentional drilling or perforation of water-bearing layers during commingled production can sometimes be unavoidable due to limited available geological information and the strong reservoir heterogeneity. The water saturation in certain layers might not be excessively high, prompting operators to aim for maximal gas production from these layers. If the pressure in the water-bearing layer surpasses that of the gas-rich layer, water might intrude into the gas-rich layer via the wellbore. (2) Interference by neighboring water-rich layer: Even when the water-rich layer is not perforated, the producing layer can still be impacted by water from an adjacent interconnected water-rich layer. Once production begins from the gas-rich layer, its pressure experiences a consistent decline. When the pressure gradient between the gas-rich and water-rich layers reaches a critical level, the water within the water-rich layer could breach barriers (such as weak joint surfaces or cement in fractures) and migrate into the gas-rich layer. (3) Interference due to wellbore-loading water during shut-in: Given that well production in tight gas reservoirs typically experiences rapid decline compared to conventional reservoirs, wells that decrease production to an uneconomical level are often temporarily shut down while awaiting secondary operations (like refracturing or workover) to restore productivity (Yu et al., 2016). During the shut-in phase, water in the wellbore is imbibed into the gas-rich layer due to capillary and hydraulic pressures. This process damages the near-well formation, a phenomenon referred to as water blockage (Andersen, 2021). After reopening the well, this damage causes the decline of the gas production or even permanently kill the well.

2.2. Insights from reservoir-scale simulation

In order to model the potential inter-layer interferences illustrated in Fig. 1, we utilize the commercial simulator IMEX developed by Computer Modeling Group to perform numerical simulations at the reservoir scale. The model comprises four primary producing layers (H8, S1, S2, and Benxi) with a vertical hydraulic fracture at each of the layer. A well is drilled at the central

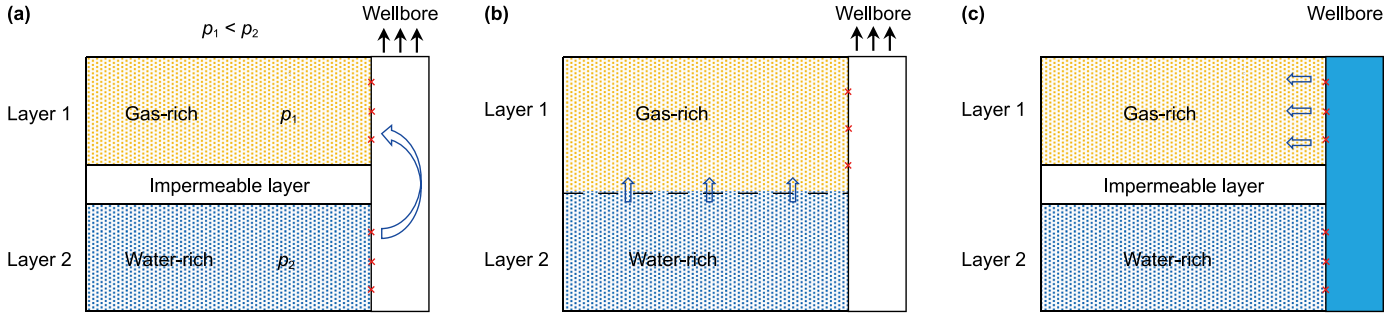

Fig. 2. Schematic diagram of inter-layer interference in the presence of water (water-rich layer) due to water invasion from perforated water-rich layer (**a**), water invasion from the neighboring connected water-rich layer (unperforated) (**b**), and water invasion from the wellbore-loading water during shut-in operation (**c**). Red cross represents perforation; blue arrow represents the flow direction of water; black arrow represents the flow direction of production fluid.

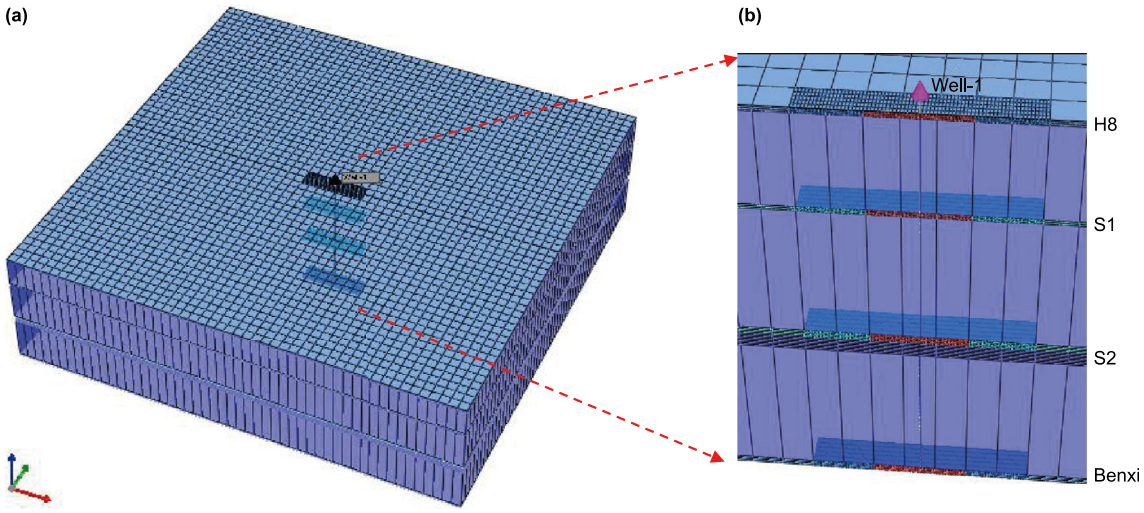

Fig. 3. (**a**) Grid structure of the reservoir-scale simulation model with four producing layers; (**b**) Local grid refinement for the vertical hydraulic fractures.

Table 1
Summary of input parameters for the four production layers during the reservoir simulation (basic case). The data are from a typical well in the Yan'an Gas Field.

Layer	Thickness, m	Matrix porosity	Permeability, mD		Pressure, MPa	Water saturation
			Matrix	Fracture		
H8	3	0.070	0.64	50	20.00	0.38
S1	3	0.078	0.91		21.28	0.42
S2	5	0.087	1.00		21.37	0.44
Benxi	4.6	0.05	0.78		25.26	0.39

point of the domain, and the fractures are symmetrically positioned on either side of the well, as depicted in Fig. 3. The dimensions of the simulation domain are 510 m (x) × 510 m (y) × 276 m (z), with detailed input data for the four layers presented in Table 1. These data are sourced from a typical well in the Yan'an Gas Field. The fracture width is 0.02 m, while its height equals the thickness of the target layer, allowing it to penetrate through the layer. To discretize the fracture space and enhance calculation stability, we implement the local grid refinement (LGR) technique. This technique is beneficial for capturing transient flow in the vicinity of the fracture region. The PVT data for dry gas (including the Z factor and gas viscosity) can be found in Zhang et al. (2017). The governing equations, capillary pressure curves (Fig. A1), and relative permeability curves (Fig. A1) for the two-phase flow simulation are provided in Appendix A. The numerical model established with single porosity/permeability has been validated and found reliable, as it has been utilized to simulate gas production and accumulation in the Yan'an tight gas reservoir in our previous works (Zhang et al., 2020; Zhao et al., 2020). It should be noted that, if the vertical fracture height is not well controlled and propagate to the upper/lower layers, additional interference will occur between the facture-connected layers, which is not considered in this work.

2.2.1. Difference in physical property

Firstly, commingled production is simulated to understand the influence of layer properties on the production performance. The original pressure of each layer is assumed as same to H8 layer (20 MPa), and the four layers are perforated for commingled

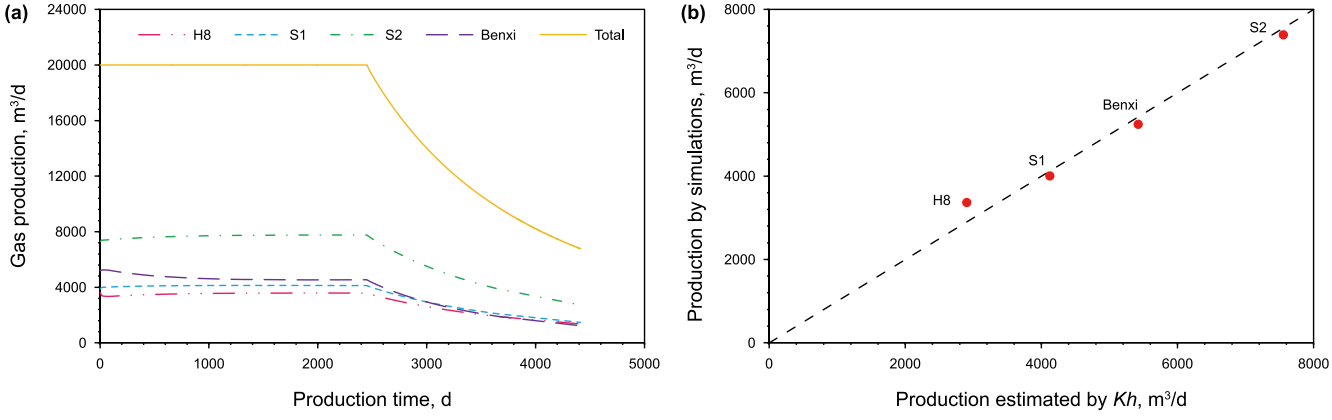

Fig. 4. Effects of difference in physical properties on the production performance. (**a**) Individual gas production and total gas production for the four producing layers; (**b**) Consistency between the production estimated by Kh and that from the simulation results. The dotted line is added to guide the reader's eye.

production at the scheme of constant gas production (20,000 m^3/d). The gas production contributed by each layer is shown in Fig. 4(a). 7 years of stable production stage can be observed under the scheme, and the production of each layer is linearly dependent on the formation coefficient *Kh* (Fig. 4(b)). The deviation of the top layer H8 and bottom layer S2 is ascribed to the difference of bottom-hole pressure for such a long vertical span (276 m). The prediction trend is consistent with the general knowledge (Lefkovits et al., 1961), which further shows the reliability of the model. Although the layer with lower *Kh* produces slower at early stage, its production starts to increase at the late stage where the pressure in the layer with higher *Kh* consumed significantly.

For the purpose of comparing commingled production with separate production, we utilize the stable production values for each layer as depicted in Fig. 4(a) to conduct individual simulations for separate production of each layer. After a 12-year production period, the recovery factor for the separate production scheme (63.44%) closely aligns with that of the commingled production scheme (62.12%). Prolonged production is expected to further minimize the difference in recovery factor. This slight difference in recovery factor can be attributed to the increased energy consumption during commingled production. Notably, although the physical properties of each layer within a multi-layer reservoir may differ, the influence of inter-layer interference during commingled production is negligible. It should be noted that, the physical properties of different layers might contribute different layer production during commingled production, while the final gas recovery factors between separate production scheme and commingled production scheme are nearly same. Therefore, we do not ascribe the physical properties of layers to inter-layer interference. Consequently, if the sole distinction between each layer lies in their physical properties, commingled production proves advantageous for engineering applications and serves to effectively reduce investment costs.

2.2.2. Multi-pressure system

In typical tight gas reservoirs, the original pressure among different layers tends to vary. When the vertical span between the top and bottom layers is considerable, the pressure disparity between these two layers can become substantial. In order to eliminate the influence of layer heterogeneity, we assume a uniform formation coefficient of 2.5 mD m for each layer. Similarly, all four layers are perforated for commingled production using a constant gas production scheme (20,000 m^3/d), where the production rate is based on the practical stable production for the well shown in Table 1 from the Yan'an Gas Field. The simulation results are presented in Fig. 5. Notably, the Benxi layer, with the highest pressure, exhibits the most substantial gas production within the initial three years (Fig. 5(a)), leading to a noticeable suppression of production in the other three layers. However, as the Benxi layer pressure declines due to production, the production contributions from the other three layers begin to rise. Considering that gas production is proportional to the square of pressure drop (Lee and Wattenbarger, 1996), the impact of layer pressure on gas production is expected to be more significant than the formation coefficient. The elevated pressure of the Benxi layer leads to quick gas production which is also favorable for its ultimate recovery factor (Fig. 5(b)). No backflow phenomenon has been observed under this production scheme. It is important to note that the lowest recovery factor for the S2 layer can be attributed to its greater reservoir volume (5 m thickness) in comparison to other layers. For the sake of comparison, simulations are also conducted using the separate production scheme. After 12 years of production, the recovery factor for the separate production scheme (59.18%) is also nearly in line with that of the commingled production scheme (57.65%).

To induce backflow, we reduce the well production constraint from 20,000−5000 m^3/d, and the simulation results are displayed in Fig. 6. During the initial production phase, only the layer with the highest pressure (Benxi) exhibits positive production, while the other three layers experience backflow (Fig. 6(a)). Due to interference, the overall gas production from the well is lower than the production from the Benxi layer alone. Remarkably, the layer with the lowest original pressure (H8) experiences a substantial initial backflow volume of up to 2000 m^3/d, which persists for nearly 2 years. This means that the H8 layer receives a consistent gas supply from the Benxi layer during the backflow stage. This supply is sufficient to increase the pressure of the H8 layer from 20 to 20.30 MPa (Fig. 6(b)). When the pressure of the Benxi layer decreases to levels comparable to the other three layers, all four layers initiate production contributions simultaneously. Parallel to the previous case, the Benxi layer pressure decline is the most rapid due to its quick production, resulting in the highest recovery factor for this layer. However, due to the prolonged backflow, the H8 layer attains the lowest recovery factor among the four layers. Following a 12-year production period, the recovery factor for commingled production stands at only 17.43% owing to the low well production constraint. Additionally, simulations are conducted using the separate production scheme, yielding a corresponding recovery factor of 25.23% for the same multi-pressure system. The substantial discrepancy in recovery factors is attributed to the severe backflow, which consumes extra energy during the inefficient gas exchange process. Consequently, inter-layer interference in this

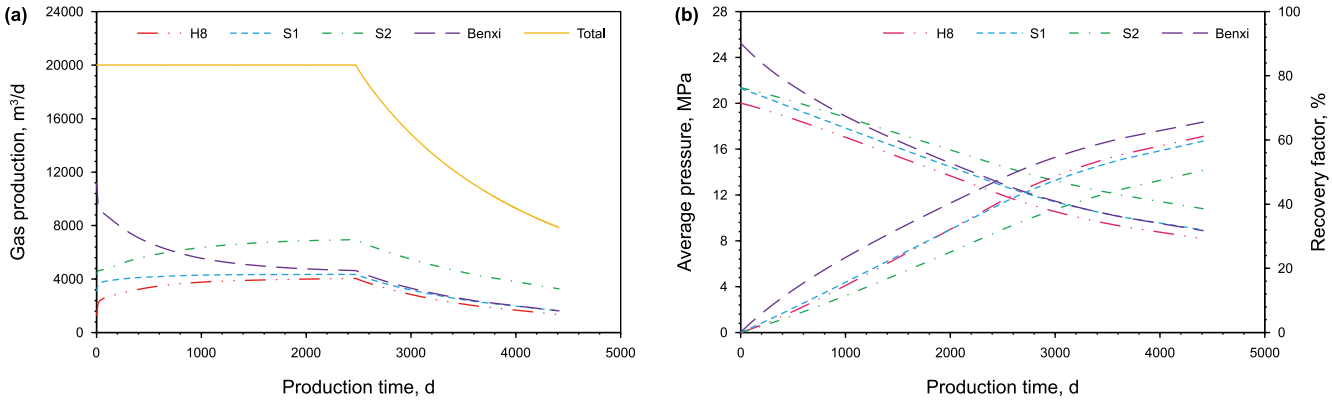

Fig. 5. Effects of multi-pressure system on the production performance (20,000 m^3/d well production constraint). (**a**) Individual gas production and total gas production for the four producing layers; (**b**) Individual gas pressure and recovery factor for the four producing layers.

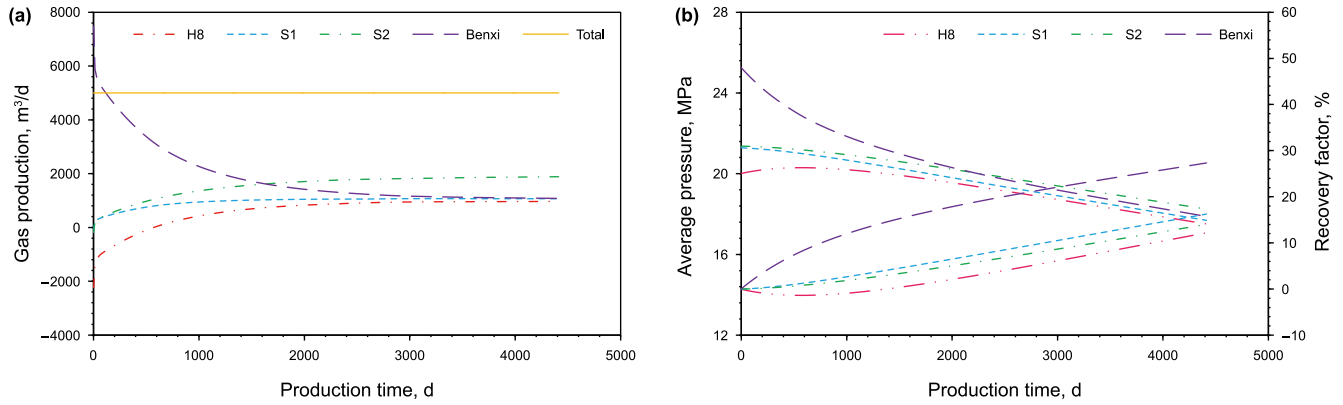

Fig. 6. Effects of multi-pressure system on the production performance (5000 m^3/d well production constraint). (**a**) Individual gas production and total gas production for the four producing layers; (**b**) Individual gas pressure and recovery factor for the four producing layers.

scenario profoundly impacts commingled production performance. Fortunately, practical field production constraints are not typically as low as used in the simulation, usually 1/3–1/5 of the open-flow capacity (Lee and Wattenbarger, 1996). As a result, the backflow phenomenon can be naturally avoided. However, if all four layers are perforated and interconnected, opting for rapid production instead of well shut-in is advisable to prevent adverse backflow occurrences.

2.3. Insights from pore-scale simulation

Reservoir-scale simulation is the optimal choice for directly observing the impacts of inter-layer interference on well production. However, when water is introduced into the multi-layer system, the intrusion of water from other layers via the wellbore (Fig. 2(a) and (c)) cannot be effectively simulated using conventional reservoir simulation methods. In this section, we employ the LBM, a pore-scale numerical tool, to visually capture water invasion and quantitatively assess its influence on gas flow capacity. LBM is recognized as the most direct mesoscopic approach for modeling multiphase flow in porous media with intricate geometries (Wang et al., 2023). To investigate inter-layer interference in the presence of water, we adopt a color-gradient LB model initially proposed by Rothman and Keller (1988), which has been further developed in the multi-relaxation-time (MRT) framework by Huang et al. (2014). Detailed information regarding the methodology is provided in Appendix B. This model has undergone careful calibration through simulations involving layered gas-water flow in a 2D channel and the injection of gas into two parallel capillary tubes with differing pore sizes, as detailed in our prior work (Zhao et al., 2021).

The geometry of the two-layer porous media is created using an algorithm known as the Voronoi tessellation technique. This algorithm divides the 2D simulation domain into numerous non-overlapping polygons using a set of random points. The lines formed by this Voronoi division are then artificially transformed into flow channels. The Voronoi tessellation technique has found wide application in generating various types of porous media, both in experimental contexts (Wu et al., 2012) and numerical simulations (Newman and Yin, 2013). The size of the flow channels within the Voronoi diagram can be controlled by the algorithm to adhere to an anticipated pore size distribution (PSD), typically derived from real tight rock. This enables the generation of porous media with varying porosities and permeabilities. By implementing different initial conditions, the three possible interference patterns in the presence of water are simulated using the porous media structures shown in Figs. 7(a), 8(a) and 9(a). The grid size of the domain is set at $760 \times 600(\Delta x^2)$, which is sufficient to visualize the interaction process between gas and water. The geometry comprises 250 seeding points, with the PSD following a truncated normal distribution function featuring an average pore size of $5\Delta x$. As a result, the reconstructed two-layer porous media possess identical porosity ($\phi = 0.231$) and equal permeability ($K = 0.540\Delta x^2$) for both layers, thereby eliminating the impact of layer properties on inter-layer interference. During the simulation, the effective gas permeability (K_g) is computed using the extended two-phase Darcy equation (Bear and Cheng, 2010). It is noteworthy that the porosity of the 2D porous media is higher than that of typical tight rock, as 2D samples require adequate connectivity to

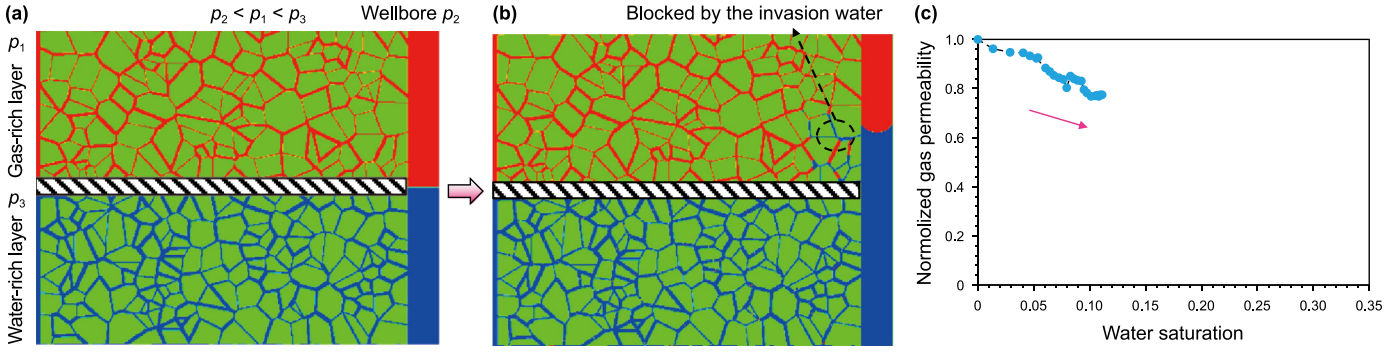

Fig. 7. Interference from perforated water-rich layer. (**a**) Initial gas/water distribution; (**b**) Gas/water distribution after 50,000 time steps; (**c**) Variation of gas effective permeability with the increase in water invasion volume for the gas-rich layer. Green = solid, red = gas, blue = water.

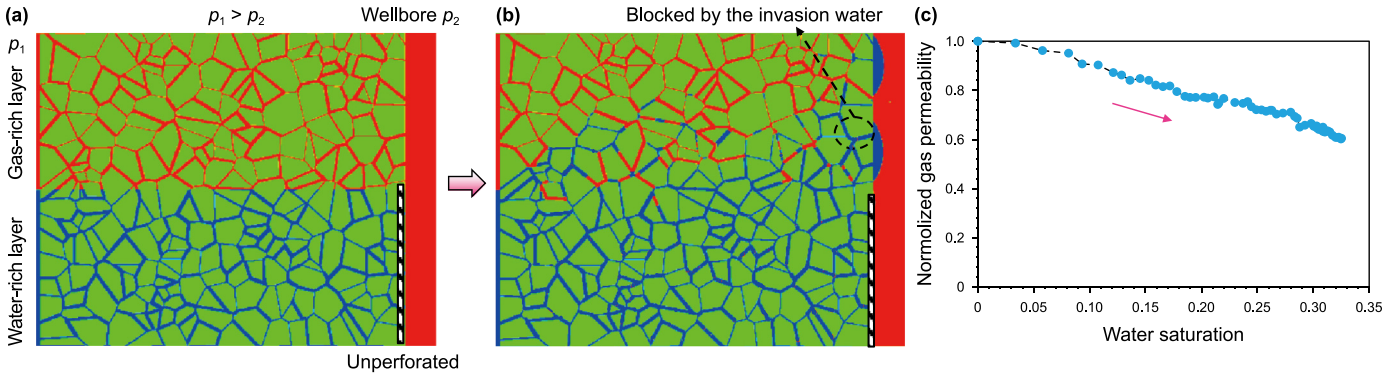

Fig. 8. Interference from unperforated water-rich layer. (**a**) Initial gas/water distribution; (**b**) Gas/water distribution after 200,000 time steps; (**c**) Variation of gas effective permeability with the increase in water invasion volume for the gas-rich layer. Green = solid, red = gas, blue = water.

facilitate flow (Zhang et al., 2021). Additionally, permeability is expressed in lattice units (Newman and Yin, 2013), and the normalized gas permeability (K_{rg}) is calculated as $K_{rg} = K_g / K$, which is employed in subsequent analyses. To reflect the reservoir conditions of the target reservoir, the density ratio of water to gas and the viscosity ratio are set at 6 and 24, respectively (Zhao et al., 2021). The wettability of the porous media is assumed to be strongly hydrophilic with a contact angle of zero.

2.3.1. Interference from perforated water-rich layer

This inter-layer interference pattern involves the intrusion of water produced from an unintentionally perforated water-rich layer into the gas layer. During the simulation, the upper gas-rich layer and the lower water-rich layer are separated by an impermeable barrier (e.g., mudrock). However, once both layers are perforated for production, they become interconnected through the wellbore. Constant boundary conditions (Zou and He, 1997) are applied to the left sides of the upper layer (p_1) and lower layer (p_3), as well as the top exit of the wellbore (p_2). The bounce-back boundary condition (Ladd, 1994) is applied to the other sides of the simulation domain. Initially, the pressure relationship among the three boundaries results in $p_2 < p_1 < p_3$, as depicted in Fig. 7(a). Upon the commencement of production, water from the lower layer ascends along the wellbore due to the pressure difference between p_3 and p_2. Simultaneously, gas from the upper layer flows into the wellbore as a result of the pressure disparity between p_1 and p_2. Because of the water-wetting characteristics of the porous media, capillary pressure comes into play when water contacts the upper gas-rich layer. In the early stages of well opening, water inevitably infiltrates the gas-rich layer under the combined influence of capillary pressure and the pressure drop between p_1 and p_3, blocking the gas effective flow pathways (Fig. 7(b)). In essence, the pressure drop between the two layers ($p_3 - p_1$) surpasses the production pressure drop ($p_3 - p_2$) due to the gradual pressure reduction as the well starts production. This imbibition phenomenon results from both capillary pressure and the multi-pressure system. If the water layer is positioned in the upper formation with lower pressure, the driving force for water infiltration is expected to be diminished. Fig. 7(c) illustrates the variation in gas effective permeability as the volume of water intrusion into the gas-rich layer increases. The gas effective permeability consistently decreases with growing water saturation. As water saturation reaches 0.11, the decrease in gas permeability halts. At this stage, gas maintains its flow pathways predominantly in the upper layer region, with the lower region largely obstructed by the invading water. A dynamic equilibrium between pressure drop ($p_1 - p_2$) and capillary pressure results in the distribution of gas and water as well as the gas effective permeability. Ultimately, the gas effective permeability drops to 0.75 of the intrinsic permeability. Here, we assumed the produced water can be effectively uplift to the ground when the gas-rich layer and water-rich layer are both perforated to production.

2.3.2. Interference from unperforated water-rich layer

The second inter-layer interference pattern involves interference from a neighboring connected water-rich layer, even if the water-rich layer itself is not perforated. In this simulation, the upper gas-rich layer and lower water-rich layer are directly connected. This physical process might occur when water from the water-rich layer breaches a weak barrier (e.g., joint surface, cement in fractures), as mentioned earlier. Constant boundary conditions are applied to the left side of both layers (p_1) and the top exit of the wellbore (p_2). The bounce-back boundary condition is used for the right side of the lower layer and other sides of the simulation domain. Essentially, the water-rich layer remains unperforated and unconnected to the wellbore. The initial pressure relationship yields $p_2 < p_1$, as depicted in Fig. 8(a). Upon initiating production, the pressure in the gas-rich layer decreases and declines. This leads to a pressure gradient between the gas-rich layer and the water-rich layer. Once this pressure gradient surpasses the threshold pressure gradient of the weak barrier, water from the lower layer ascends to the gas-rich layer due to the combined influence of the pressure gradient and capillary pressure, as illustrated in Fig. 8(b). The invasion of external water disrupts the original flow pathways of the gas phase, resulting in nearly linear reduction of gas effective permeability with increasing water intrusion volume (Fig. 8(c)). Upon reaching dynamic balance, the invaded water saturation in the gas-rich layer reaches 0.34, and the corresponding gas effective permeability drops to 0.58 of the intrinsic permeability. During the dynamic-balance stage, gas tends to flow through the larger pores in the upper region of the layer, while the pores in the lower region are largely occupied by invading water.

Actually, this type of interference is similar to the water coning phenomenon that occurs in conventional gas reservoirs. When a production well partially penetrates the main producing zone with underlying water, the gas/water contact forms a rising conical

shape up to the wellbore (Muskat and Wycokoff, 1935). In such cases, the rising of the gas/water contact is determined by the balance between viscous force and net gravity force. Numerous analytical and empirical models have been introduced to predict the critical rate and optimize the wellbore penetration depth, thus achieving an extended period of water-free production (Tabatabaei et al., 2012). Therefore, we have developed a reservoir-scale numerical model to illustrate the potential of partial penetration in mitigating water intrusion from the unperforated layer. As evidenced by the simulations depicted in Fig. C1 (Appendix C), reducing the perforation thickness of the gas-rich layer does not enhance gas production, and water continues to ascend to the gas-rich layer, impacting gas production. This phenomenon arises from the dominance of capillary forces in tight reservoirs, where fluid flow is primarily governed by capillary force, while the influences of gravity and viscous forces are negligible. The movement of water is dictated by the ganglion dynamics of the gas/water two-phase flow, a phenomenon greatly influenced by the pore structure and wettability of the porous media (Singh et al., 2016; Li et al., 2018). Furthermore, gas layers in tight gas reservoirs tend to have relatively thin thickness (5 m in the studied well), leading to significant costs associated with productivity loss from unperforated sections. As a result, once the gas-rich layer and underlying water-rich layer are interconnected, efforts to control production rates or utilize partial perforation are not workable, and water production becomes inevitable.

2.3.3. Interference from shut-in induced imbibition

The final pattern of inter-layer interference involves that the gas layer is interfered by the wellbore-loading water during shut-in operation. When the gas flow rate falls below the minimum unloading gas flow rate, produced water tends to accumulate at the bottom of the wellbore. The boundary conditions resemble those depicted in Fig. 7(a), with equal pressures at each boundary, i.e., $p_1 = p_2 = p_3$, as shown in Fig. 9(a). In the initial state, the wellbore is fully saturated with produced water. During the shut-in period, the water in the wellbore spontaneously imbibes into the gas-rich layer due to its water-wetting nature (Fig. 9(b)). Pores in the vicinity of the wellbore become completely blocked by the invading water, causing the effective gas permeability of the layer to drop to zero rapidly. When production resumes, gas has to overcome the water-saturated pores to reach the wellbore, leading to a sudden surge in gas effective permeability (Fig. 9(c)). As production continues, the invaded water is gradually produced out of the porous media. Nonetheless, complete removal of the invaded water is not possible due to the strong surface absorption of pores (Li et al., 2017) and potential phase trapping during two-phase flow (Singh et al., 2016). In this simulated case, an invaded water saturation of 0.31 diminishes only to 0.14 after long gas drainage time, and the effective gas permeability only recovers to 0.42 of the original permeability. In comparison to the previous two interference patterns, the interference during shut-in operations is the most severe because it completely obstructs gas flow pathways. If the previous two types of interference are to encounter well shut-in operations, the interference will become increasingly worse. It is important to note that the pore-scale simulation does not consider clay damage such as swelling and migration, leading to an underestimation of the water-blockage effect. Conversely, initial water saturation usually exists in the gas-rich layer, and disregarding this initial water saturation overestimates the water-blockage effect due to the dependence of capillary pressure on water saturation.

To sum up, among the five possible types of inter-layer interferences, the inter-layer interference caused by the difference in physical properties of each layer during commingled production is negligible. However, engineers should pay much attention to the other four types of inter-layer interferences which might significantly influence the gas production.

3. Field evidences

In this section, several typical gas wells from Yan'an Gas Field are selected to support the findings and conclusions in the previous sections. Yan'an Gas Field, located in the southern Ordos Basin (China), is a typical tight gas reservoir with porosity and permeability ranges from 2.5% to 6% and 0.01 to 3 mD, respectively. From top to bottom, four gas-rich layers including H8, S1, S2 and Benxi are generally developed in the field. Due to the continental geological setting of the reservoir, the gas field exhibits poor permeability, thin layer thickness, and low lateral continuity (Zhang et al., 2020), and the strategy of commingled production is frequently adopted to increase the single-well production for this multi-layer tight gas reservoir.

3.1. Gas production without water

3.1.1. Difference in physical property

Well A-1 is a development well which was hydraulically fractured and started to production in June 2014, and the average daily gas production is 8200 m^3/d. Total numbers of three layers (H8, S1, and S2) are perforated to have commingled production for this gas well. The initial water saturations of the three layers are in the range of 56%–61%, which is generally close to the irreducible water saturation of these layers. The production data also indicate that the production water is mostly from the condensate water. The

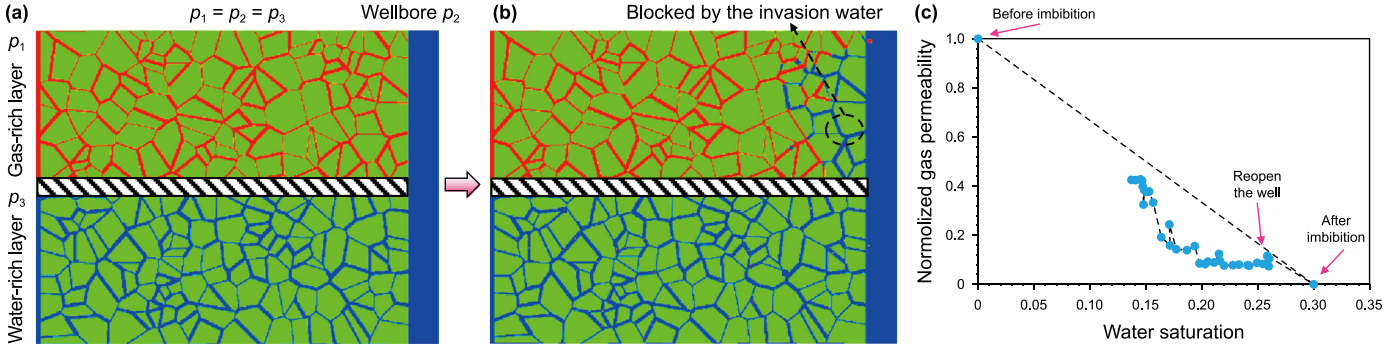

Fig. 9. Interference from shut-in induced imbibition. (**a**) Initial gas/water distribution; (**b**) Gas/water distribution after 200,000 time steps (at the end of imbibition); (**c**) Relationship between gas effective permeability and the water saturation for the gas-rich layer (before imbibition, after imbibition, and well reopening). Green = solid, red = gas, blue = water.

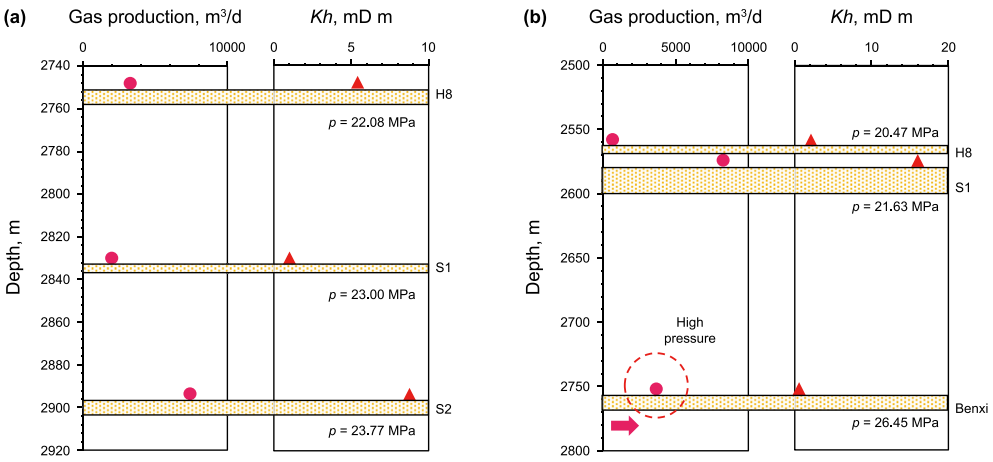

Fig. 10. Production profile testing to show the production contribution of each layer with difference in physical property but nearly same pressure system (Well A-1) (**a**), and influenced by multi-pressure system (Well A-2) (**b**). Yellow dotted strip indicates the location and thickness of producing layer.

initial pressure of the three layers is also nearly similar (maximum difference of 1.7 MPa) due to relatively close distance between each of them. Therefore, the gas production of each layer for the dry gas well is solely related to its physical property. A production profile testing conducted in October 2018 (Fig. 10(a)) shows that the gas production of each layer is closely proportional to the formation coefficient *Kh*. The trend validated the reservoir-scale simulation results, providing the basic principle for the following comparisons where the inter-layer interference occurs.

3.1.2. Multi-pressure system

Well A-2 is another development well that was hydraulically fractured and initiated production in September 2014, with an average daily gas production of 12000 m^3/d. Commingle production is achieved by perforating three layers from top to bottom: H8, S1, and Benxi. The initial water saturations of these three layers (ranging from 52% to 55%) are in proximity to their irreducible water saturation levels, and no formation water except for condensate water, with an average daily production of 0.2 m^3/d, has been recorded. However, due to the significant vertical distance between the Benxi layer and the other two layers (over 175 m), the initial pressure of the Benxi layer is 5 MPa higher than that of the other layers. Consequently, the gas production from each layer in this well does not exhibit a linear relationship with its formation coefficient *Kh*. This can be observed in the results of the production profile test conducted in October 2017 (Fig. 10(b)). Considering the linear correlation between gas production of a layer and its *Kh*, the gas production of the Benxi layer with a *Kh* of 0.28 mD m should theoretically be below 500 m^3/d. However, its actual gas production exceeds 2500 m^3/d due to its high-pressure conditions. Referring to the simulation outcomes depicted in Fig. 5, the Benxi layer, possessing the highest pressure, suppresses the production from the other layers for the first several years. Especially, the gas production for H8 layer is nearly 650 m^3/d owing to the interference, although the ultimate recovery factor of for the commingled production in comparison with separate production is expected to be minimal, as we indicated before.

3.2. Gas production with water

3.2.1. Interference from perforated water-rich layer

Well B-1 is a representative well where production is impacted by the perforated water-rich layer. This well commenced production in November 2011, with an average daily gas production of 21,000 m^3/d. The gas well encompasses three producing layers: H8, S2, and Benxi. Among these, H8 and S2 are gas-rich layers, while Benxi is a water-rich layer with an initial water saturation of 0.67, exceeding the irreducible water saturation of 0.45. Additionally, the Benxi layer has the highest initial pressure (24.34 MPa) ascribed to its bottom location, and the initial pressures of H8 and S2 are 20.15 and 22.53 MPa, respectively. As depicted in Fig. 11(a), despite its low *Kh* value (0.3), the Benxi layer significantly contributes to gas production (2955 m^3/d) due to its high initial pressure. When the three layers are perforated concurrently for production, the water produced from the high-pressure Benxi layer migrates upwards to the low-pressure H8 layer during the initial production stage. This migration results in water blockage and a decrease in effective gas permeability of the H8 layer, aligning with the indications in Fig. 7. As a result, the production profile testing conducted in October 2017 shows negligible gas contribution of the H8 layer. The pores in the near-well region of the H8 layer are blocked by the invaded water, and this scenario is particularly pronounced in tight formations. Conversely, due to the relatively high permeability and substantial pressure of the S2 layer, no invasion damage has been observed. Fig. 11(b) illustrates the production data for well B-1, showcasing a continuous and stable water production (averaging 2.1 m^3/d) attributed to the perforation of the Benxi layer. Hence, the inter-layer interference resulting from the perforated water-rich layer and the unequal pressure system significantly impacts the recovery of the gas-rich layer.

3.2.2. Interference from unperforated water-rich layer

Gas production interfered from unperforated water-rich layer is a very interesting case for tight sandstone reservoir in Yan'an Gas Field. Well B-2, which commenced production in November 2018 with an average daily gas production of 6300 m^3/d, serves as a typical example. This is also a three-layer commingled production well, involving the H8, S1, and Benxi layers. During the reservoir evaluation, the well logging data reveal that all three layers qualify as gas-rich ones, characterized by initial water saturations ranging from 0.37 to 0.41 (Fig. 12(a)), slightly below or approximately equivalent to the irreducible water saturation. Namely, except the condensed water, the three layers are supposed to produce single phase gas. Nevertheless, the consistent water production of nearly 1 m^3/d has led to the conclusion that mobile formation water is being produced from this gas well, as highlighted in Fig. 12(b). It is important to note that a water gas ratio exceeding 1 (m^3/d)/(10^4 m^3/d) is considered the critical threshold for production of

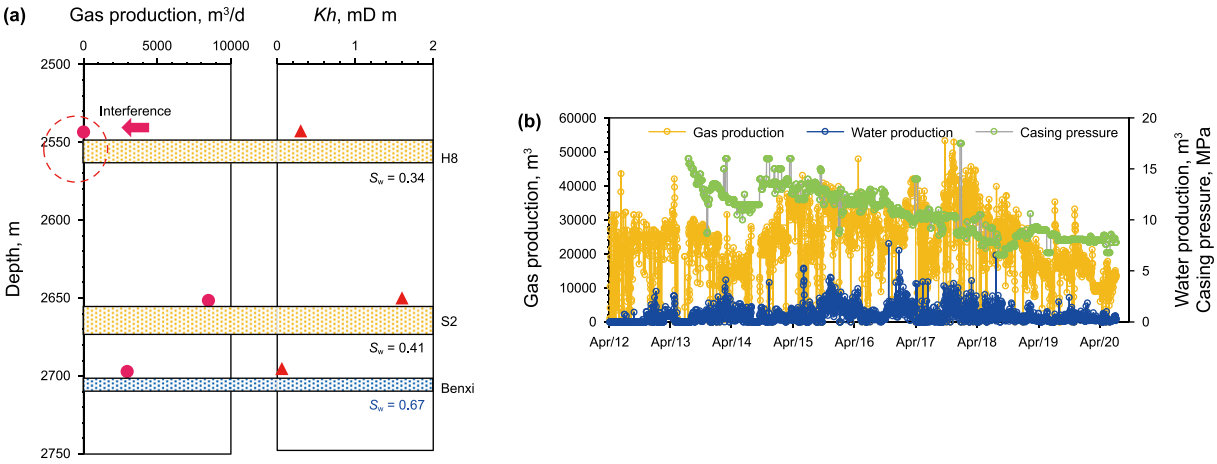

Fig. 11. (**a**) Production profile testing to show the production contribution of each layer resulting from the interference of perforated water-rich layer (well B-1); (**b**) Production data for well B-1. Yellow dotted strip indicates the location and thickness of gas-rich layer; blue dotted strip indicates the location and thickness of water-rich layer.

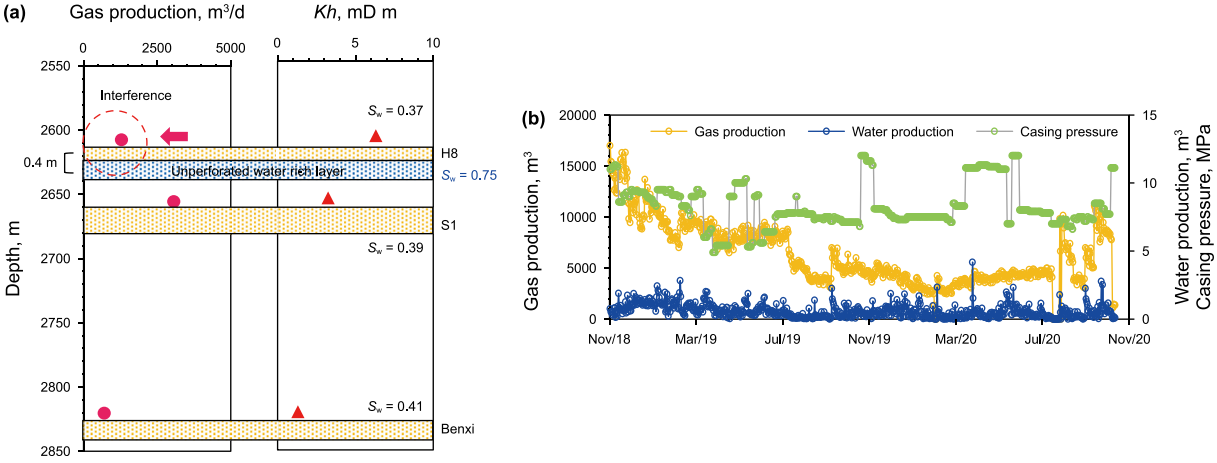

Fig. 12. (**a**) Production profile testing to show the production contribution of each layer resulting from the interference of unperforated water-rich layer (well B-2); (**b**) Production data for well B-2. Yellow dotted strip indicates the location and thickness of gas-rich layer; blue dotted strip indicates the location and thickness of water-rich layer.

formation water. Following a meticulous examination of the well logs, a coal seam with water saturation up to 0.75 was identified beneath the H8 layer. This coalbed seam was separated from the H8 layer by a 0.4-m-thick mudrock that acted as a flow barrier. As elaborated upon in Fig. 8, once the pressure gradient has exceeded the threshold pressure gradient for the barrier, the water within the water-rich layer (in this case, the coalbed seam) can permeate into the gas-rich layer, coexisting with the gas and contributing to production. Given the superior petrophysical characteristics of the H8 layer compared to the other two producing layers, the invading

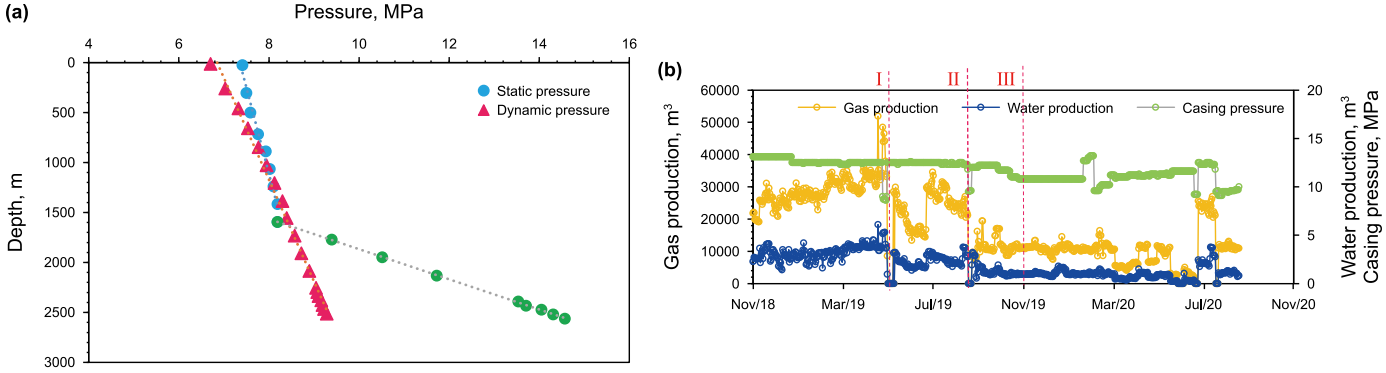

Fig. 13. (**a**) Production pressure testing results during the well shut-in (static pressure) and after the reopening operation (dynamic pressure) for well B-2; (**b**) Production data for well B-2 to show the production interfered by shut-in induced imbibition. The point I is the time to shut in the well due to the surface pipeline problem; point II is the time to conduct static pressure test; point III is the time to conduct dynamic pressure test.

water shifted the flow regime from a single gas phase to a gas/water two-phase configuration for this layer. This transformation notably impacted the gas production of the well. Actually, coalbed seams with abundant original water widely coexist with the tight gas layers in Ordos basin, China (Yang et al., 2012; Zaini et al., 2019). Well B-2 stands as a typical example of a gas well influenced by an unperforated water-rich layer, and many similar gas wells can be identified within Yan'an Gas Field. Consequently, in the process of selecting perforation layers, attention must not solely focus on the physical attributes of the primary producing layers. Rather, careful evaluation of the barrier separating the producing layer from neighboring water-rich layers is imperative to avoid potential water breakthroughs and formation damage.

3.2.3. Interference from shut-in induced imbibition

Well B-3 represents a typical case in which production is influenced by the imbibition caused by shut-in operations. The well commenced production in November 2018, as depicted in Fig. 13. It involves two producing layers, namely H8 and S1. The H8 layer is characterized by a relatively high initial water saturation of 0.66, classifying it as a water-rich layer, while the S1 layer is a gas-rich one with an initial water saturation of 0.45. Both layers are perforated to enable commingled production. During the initial half-year of production, the well demonstrated strong performance with an average daily gas production of 28,000 m^3/d. However, as illustrated in Fig. 13(b), a 10-day closure occurred in May 2019 (point I) due to surface pipeline issues. Subsequent reopening of the well resulted in a sharp reduction in gas production to 15,000 m^3/d. In September (point II), a shut-in period was imposed for pressure testing (static pressure), revealing two distinct pressure gradient lines in Fig. 13(a). This disparity indicated the gravitational separation of gas and water at a depth of 1595 m during this shut-in interval. Upon reopening, gas production further decreased to 10,000 m^3/d. In November (point III), another pressure test (dynamic pressure) was conducted, suggesting that water could be effectively lifted to the ground surface during production. Traditionally, in tight and shale gas reservoirs, an extended shut-in period leads to improved gas rates upon resuming production due to pressure buildup and the alleviation of water blocking (Cheng, 2012). However, in this case, the gas production exhibited substantial declines following well reopening, and the primary explanation lies in the interference resulting from shut-in-induced imbibition. Throughout the two shut-in periods, water produced from the H8 layer accumulated at the wellbore bottom due to gravitational differentiation. During these periods, capillary forces and hydraulic pressure drive the imbibition of water into the gas-rich layer, obstructing gas flow pathways and reducing gas permeability. Consequently, when a gas-rich layer serves as the principal production layer while water production from other layers simultaneously occurs, it is advisable to minimize shut-in operations to protect the gas flow pathways within the gas-rich layer.

4. Conclusions

(1) When no water is being produced from the multi-layer tight gas reservoir, the production performance of separate production or commingled production for layers with different physical properties is nearly the same. In reservoirs with a multi-pressure system, the backflow phenomenon, only occurs in extreme conditions (e.g., very low production rates or well shut-in). During normal production operations, the backflow has a negligible effect on production performance, and commingled production remains favorable.

(2) When a gas-rich layer is produced together with a water-rich layer, water from the water-rich layer can invade into the gas-rich layer through the wellbore. This invasion of water would block gas flow pathways and reduce effective gas permeability (decreasing it to 0.75 of the intrinsic permeability in the case). Perforating both the gas-rich layer and the water-rich layer for commingled production should be avoided.

(3) When the gas-rich layer is perforated for production, water from the neighboring water-rich layer may breach barriers such as weak joint surfaces or cement in fractures, migrating into the gas-rich layer and damaging its gas permeability. Traditional methods like production rate control or partial perforation are not effective here due to strong capillary pressure and typically thin layer thickness. Careful evaluation of the barrier is necessary to prevent potential water breakthrough.

(4) If a gas-rich layer is the primary producing layer and there is simultaneous water production from other layers, the water remains at the bottom of the wellbore can be imbibed into the gas-rich layer under the influence of capillary force and hydraulic pressure, causing damage to the near-well formation. This results in reduced gas production when the well is reopened. In such a situation, shut-in operations should be minimized as much as possible.

CRediT authorship contribution statement

Tao Zhang: Investigation, Conceptualization. **Bin-Rui Wang:** Software, Investigation. **Yu-Long Zhao:** Writing – original draft, Investigation. **Lie-Hui Zhang:** Supervision, Funding acquisition. **Xiang-Yang Qiao:** Resources, Formal analysis, Data curation. **Lei Zhang:** Visualization, Validation, Methodology. **Jing-Jing Guo:** Writing – review & editing, Methodology. **Hung Vo Thanh:** Writing – review & editing, Methodology.

Declaration of competing interest

The authors declare that they have no known competing financial interests or personal relationships that could have appeared to influence the work reported in this paper.

Acknowledgments

This work is supported by the National Natural Science Foundation of China (Grant Nos. 52304044, 52222402, 52234003, 52174036), Sichuan Science and Technology Program (Nos. 2022JDJQ0009, 2023NSFSC0934), Key Technology R&D Program of Shaanxi Province (2023-YBGY-30), the Science and Technology Cooperation Project of the CNPC-SWPU Innovation Alliance (Grant No. 2020CX030202), and the China Postdoctoral Science Foundation (Grant No. 2022M722638). The authors would also like to thank Computer Modeling Group (CMG) for their simulation software.

Appendix A

For gas/water two-phase flow under isothermal process, the fluid flow equation can be expressed as follow (Peaceman, 1997):

$$\frac{\partial}{\partial t}(\nabla S_\sigma \rho_\sigma \phi) + \nabla(\rho_\sigma v_\sigma) + q_\sigma = 0, \tag{A-1}$$

where the subscript σ represents gas or water phase; S is

saturation; ρ is density; ϕ is the reservoir porosity; v is the volumetric velocity vector; q is the sink or source term per unit volume of formation.

Fluid flow in matrix is described by Darcy's law, which can be described as

$$v_i = \frac{KK_{\mathrm{ri}}}{\mu_i}\nabla p, \tag{A-2}$$

where ∇p is the pressure drop; μ is the fluid viscosity; K is the intrinsic permeability; K_{r} is the relative permeability.

In the fracture, nonlinear equation between pressure drop and fluid velocity by using Forchheimer number is used to characterize the non-Darcy flow at high velocity, written as

$$-\nabla p = \frac{\mu_i}{K_i}v_i + \beta_i\rho_i v_i^2, \tag{A-3}$$

where β can be calculated by (Frederick and Graves, 1994) Eq. (A-4):

$$\beta = \frac{6.923\times 10^{10}}{(KK_{\mathrm{ri}})^{1.55}}. \tag{A-4}$$

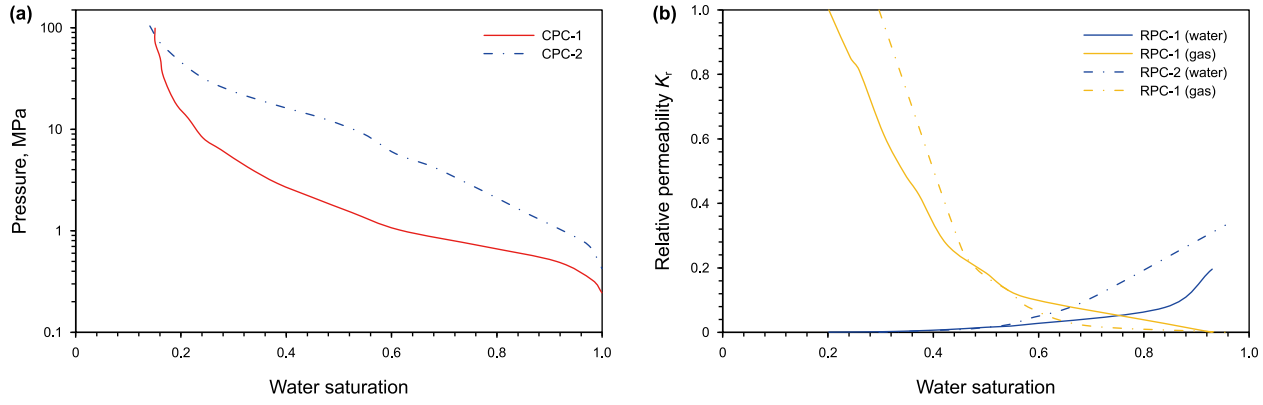

Fig. A1. Capillary pressure curves (CPC) obtained through mercury injection test and relative permeability curves (RPC) obtained through drainage test are input into the numerical simulations. CPC-1 and RPC-1 are used in H8 and Benxi layers; CPC-2 and RPC-2 are used in S1 and S2 layers.

Appendix B

In color-gradient model, two-particle distribution functions $f_i^r(x,t)$ and $f_i^b(x,t)$ are defined, where superscripts r and b represent the red component and blue component. In one calculation loop, besides the streaming and collision in single-phase LBM, an additional step named recoloring is implemented in the color-gradient model. Here, the evolution of the particle-distribution function is given by (Rothman and Keller, 1988)

$$f_i^{\sigma}(\boldsymbol{x}+\boldsymbol{e}_i\Delta t, t+\Delta t) = f_i^{\sigma}(\boldsymbol{x},t) + (\Omega_i^{\sigma})^1 + (\Omega_i^{\sigma})^2, \tag{B-1}$$

where $f_i^{\sigma}(\boldsymbol{x},t)$ is the nonequilibrium distribution function; Δt is a time step; $\boldsymbol{e}_i$ is lattice discrete velocity; $(\Omega_i^{\sigma})^1$ and $(\Omega_i^{\sigma})^2$ are two collision terms. The MRT collision operator instead of SRT is adopted in this work, which can enhance the numerical stability of the regular color-gradient model. The collision term $(\Omega_i^{\sigma})^1$ in the form of MRT can be represented by (Huang et al., 2014)

$$(\Omega_i^{\sigma})^1 = -M^{-1}\widehat{\boldsymbol{S}}\left[|m(\boldsymbol{x},t)\rangle - \left|m^{(\mathrm{eq})}(\boldsymbol{x},t)\right\rangle\right], \tag{B-2}$$

where $|\cdot\rangle$ is Dirac notion, representing column vectors; $\widehat{\boldsymbol{S}}$ is a diagonal with $\widehat{\boldsymbol{S}} = \mathrm{diag}(s_0,s_1,s_2,s_3,s_4,s_5,s_6,s_7,s_8)$; $|m\rangle$ and $|m^{(\mathrm{eq})}\rangle$ are vectors of moments; M is a linear transformation matrix, which is used to map the vector $|f\rangle$ in velocity space to the vector $|m\rangle$ in moment space: $|m\rangle = M\cdot|f\rangle$.

The correction form of the second collision term $(\Omega_i^{\sigma})^2$ is written as (Reis and Phillips, 2007)

$$(\Omega_i^{\sigma})^2 = \frac{A_{\sigma}}{2}|\boldsymbol{f}|\left[\omega_i\frac{(\boldsymbol{e}_i\cdot\boldsymbol{f})^2}{|\boldsymbol{f}|^2} - B_i\right], \tag{B-3}$$

where the color gradient $\boldsymbol{f}$ can be shown as (Latva-Kokko and Rothman, 2005)

$$\boldsymbol{f}(\boldsymbol{x},t) = \sum_i \boldsymbol{e}_i\sum_j\left[f_j^r(\boldsymbol{x}+\boldsymbol{e}_i\Delta t,t) - f_j^b(\boldsymbol{x}+\boldsymbol{e}_i\Delta t,t)\right]. \tag{B-4}$$

To obtain phase separation, the recoloring step shown as follows is employed in the color-gradient LBM (Latva-Kokko and Rothman, 2005)

$$f_i^{r+}(\boldsymbol{x},t) = \frac{\rho_r}{\rho}f_i^* + \beta\frac{\rho_r\rho_b}{\rho^2}f_i^{\mathrm{eq}}(\rho,\boldsymbol{u}=0)\cos(\lambda_i), \tag{B-5}$$

$$f_i^{b+}(\boldsymbol{x},t) = \frac{\rho_b}{\rho}f_i^* - \beta\frac{\rho_r\rho_b}{\rho^2}f_i^{\mathrm{eq}}(\rho,\boldsymbol{u}=0)\cos(\lambda_i), \tag{B-6}$$

where β is also related to interfacial properties. The bounce-back boundary condition is implemented to achieve no slip at the solid surface (Ladd, 1994). More detailed information of the used model including the values of the above parameters can refer to Huang et al. (2014).

Appendix C

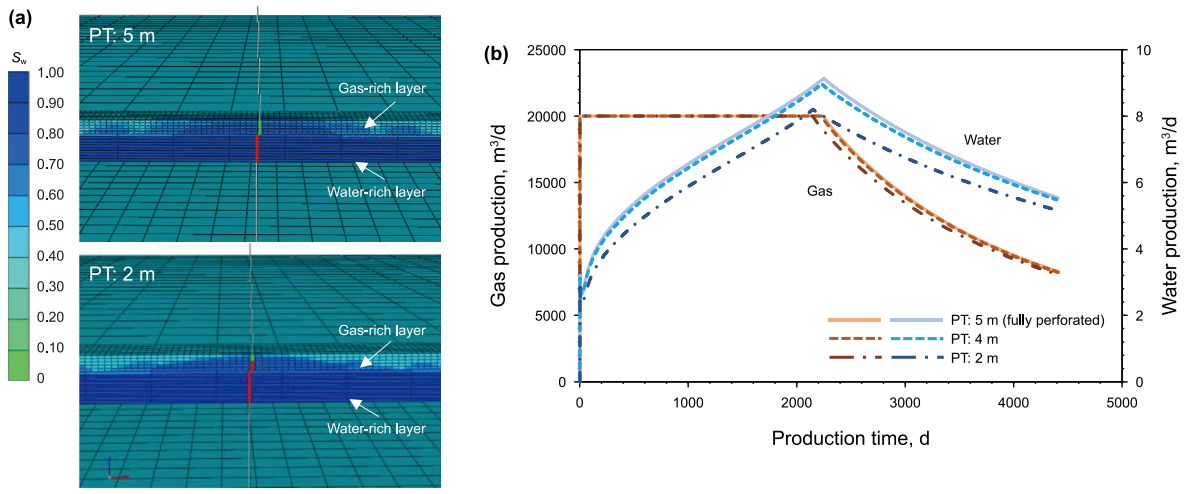

Fig. C1. (**a**) Section view to show water invasion from the bottom connected water-rich layer under different perforation thickness (PT); (**b**) Gas and water daily production under different perforation thickness. The thickness of the layer is 5 m.

References

Andersen, P.O., 2021. Steady-state gas flow from tight shale matrix subject to water blocking. SPE J. 26 (6), 3970–3985. https://doi.org/10.2118/202337-PA.

Bear, J., Cheng, A.H.D., 2010. Modeling Groundwater Flow and Contaminant Transport. Springer Dordrecht Heidelberg London, New York.

Bennion, D.B., Thomas, F.B., 2005. Formation damage issues impacting the productivity of low permeability, low initial water saturation gas producing formations. J. Energy Resour. Technol. 127 (3), 240–247. https://doi.org/10.1115/1.1937420.

BGR (Federal Institute for Geosciences and Natural Resources), 2014. Energy Study 2014: Reserves, Resources and Availability of Energy Resources.

BP (British Petroleum Company), 2018. BP Statistical Review of World Energy. BP. https://www.bp.com/bp-stats-review-2018-full-report.pdf.

Cheng, Y., 2012. Impact of water dynamics in fractures on the performance of hydraulically fractured wells in gas-shale reservoirs. J. Can. Petrol. Technol. 51 (2), 143e151. https://doi.org/10.2118/127863-PA.

Cox, S.A., Stoltz, R.P., Wilson, A.S., Sutton, R.P., 2003. Reserve analysis for multilayered tight gas reservoirs. In: SPE Eastern Regional Meeting, Pittsburgh, Pennsylvani. https://doi.org/10.2118/84814-MS.

Eisa, M., Kumar, A., Zaouali, Z., Chaabouni, H., Al-Ghadbhan, H., Kadhim, F., 2013. Integrated workflow to evaluate and understand well performance in multi layer mature gas reservoirs Bahrain case study. In: SPE Middle East Oil and Gas Show and Conference, Manama, Bahrain. https://doi.org/10.2118/164356-MS.

El-Banbi, A.H., Wattenbarger, R.A., 1996. Analysis of commingled tight gas reservoirs. In: SPE Annual Technical Conference and Exhibition, Denver, Colorado. https://doi.org/10.2118/36736-MS.

El-Banbi, A.H., Wattenbarger, R.A., 1997. Analysis of commingled gas reservoirs with variable bottom-hole flowing pressure and non-Darcy flow. In: SPE Annual Technical Conference and Exhibition, San Antonio. https://doi.org/10.2118/38866-MS.

Frederick, D., Graves, R., 1994. New correlations to predict non-Darcy flow coefficients at immobile and mobile water saturation. In: SPE Annual Technical Conference and Exhibition, New Orleans, Louisiana, USA. https://doi.org/10.2118/28451-MS.

He, D., Jia, A., Ji, G., Wei, Y., Tang, H., 2013. Well type and pattern optimization technology for large scale tight sand gas, Sulige Gas Field, NW China. Petrol. Explor. Dev. 40 (1), 84–95. https://doi.org/10.1016/S1876-3804(13)60008-7.

Huang, H., Huang, J.J., Lu, X.Y., 2014. Study of immiscible displacements in porous media using a color-gradient-based multiphase lattice Boltzmann method. Comput. Fluids 93 (8), 164–172. https://doi.org/10.1016/j.compfluid.2014.01.025.

IEA (International Energy Agency), 2017. Outlook for Natural Gas. IEA. http://www.iea.org//WEO2017Excerpt_Outlook_for_Natural_Gas.pdf.

Jiang, L., Zhao, W., Bo, D., Hong, F., Gong, Y., Hao, J., 2023. Tight sandstone gas accumulation mechanisms and sweet spot prediction, Triassic Xujiahe Formation, Sichuan Basin, China. Petrol. Sci. 2023. https://doi.org/10.1016/j.petsci.2023.07.008.

Juell, A., Whitson, C.H., 2011. Backpressure equation for layered gas reservoirs. In: SPE Annual Technical Conference and Exhibition, Denver, Colorado, USA. https://doi.org/10.2118/146066-MS.

Kuppe, F., Chugh, S., Connell, P., 2000. Material balance for multi-layered, commingled, tight gas reservoirs. In: SPE/CERI Gas Technology Symposium, Calgary, Alberta, Canada. https://doi.org/10.2118/59760-MS.

Ladd, A.J., 1994. Numerical simulations of particulate suspensions via a discretized Boltzmann equation. Part 1. Theoretical foundation. J. Fluid Mech. 271 (1), 285–309. https://doi.org/10.1017/S0022112094001771.

Latva-Kokko, M., Rothman, D., 2005. Static contact angle in lattice Boltzmann models of immiscible fluids. Phys. Rev. E 72 (4), 046701. https://doi.org/10.1103/PhysRevE.72.046701.

Lee, J., Wattenbarger, R., 1996. Gas Reservoir Engineering. Society of Petroleum Engineers.

Lefkovits, H.C., Hazebroek, P., Allen, E.E., Matthews, C.S., 1961. A study of the behavior of bounded reservoirs composed of stratified layers. Soc. Petrol. Eng. J. 1 (1), 43–58. https://doi.org/10.2118/1329-G.

Li, J., Li, X., Wu, K., Feng, D., Zhang, T., Zhang, Y., 2017. Thickness and stability of water film confined inside nanoslits and nanocapillaries of shale and clay. Int. J. Coal Geol. 179, 253–268. https://doi.org/10.1016/j.coal.2017.06.008.

Li, Z., Galindo-Torres, S., Yan, G., Scheuermann, A., Li, L., 2018. A lattice Boltzmann investigation of steady-state fluid distribution, capillary pressure and relative permeability of a porous medium: effects of fluid and geometrical properties. Adv. Water Resour. 116, 153–166. https://doi.org/10.1016/j.advwatres.2018.04.009.

Liu, G., Meng, Z., Luo, D., Wang, J., Gu, D., Wang, D., 2020. Experimental evaluation of interlayer interference during commingled production in a tight sandstone gas reservoir with multi-pressure system. Fuel 262, 116557. https://doi.org/10.1016/j.fuel.2019.116557.

Liu, H., Pang, J., Wang, X., Yu, X., Li, Q., 2012. Analysis of interlayer interference and research of development strategy of multilayer commingled production gas reservoir. Energy Proc. 16, 1341–1347. https://doi.org/10.1016/j.egypro.2012.01.214.

Milad, B., Civan, F., Devegowda, D., Sigal, R.F., 2013. Modeling and simulation of production from commingled shale gas reservoirs. In: SPE/AAPG/SEG Unconventional Resources Technology Conference, Denver, Colorado. https://doi.org/10.1190/urtec2013-061.

Muskat, M., Wycokoff, R.D., 1935. An approximate theory of water-coning in oil production. OR Trans. 114 (1), 144–163. https://doi.org/10.2118/935144-G.

Newman, M.S., Yin, X., 2013. Lattice Boltzmann simulation of non-Darcy flow in stochastically generated 2D porous media geometries. SPE J. 18 (1), 12–26. https://doi.org/10.2118/146689-PA.

Peaceman, D.W., 1997. Fundamentals of Numerical Reservoir Simulation. Elsevier Scientific Publisching Co.

Qiao, J., Zeng, J., Jiang, S., Zhang, Y., Feng, S., Feng, X., Hu, H., 2020. Insights into the pore structure and implications for fluid flow capacity of tight gas sandstone: a case study in the Upper Paleozoic of the Ordos Basin. Mar. Petrol. Geol. 118, 104439. https://doi.org/10.1016/j.marpetgeo.2020.104439.

Rahman, N.M.A., Mattar, L., 2007. New analytical solution to pressure transient problems in commingled, layered zones with unequal initial pressures subject to step changes in production rates. J. Pet. Sci. Eng. 56 (4), 283–295. https://doi.org/10.1016/j.petrol.2006.10.002.

Reis, T., Phillips, T.N., 2007. Lattice Boltzmann model for simulating immiscible two-phase flows. J. Phys. Math. Theor. 40 (14), 4033–4053. https://doi.org/10.1088/1751-8113/40/14/018.

Rothman, D.H., Keller, J.M., 1988. Immiscible cellular-automaton fluids. J. Stat. Phys. 52 (3–4), 1119–1127. https://doi.org/10.1007/BF01019743.
Shanley, K.W., Cluff, R.M., Robinson, J.W., 2004. Factors controlling prolific gas production from low-permeability sandstone reservoir: implications for resources assessment, prospect development, and risk analysis. APPG Bulletin 88 (8), 1083–1121. https://doi.org/10.1306/03250403051.
Shaoul, J., Zelm, L.V., Pater, C.J., 2011. Damage mechanisms in unconventional-gas-well stimulation—a new look at an old problem. SPE Prod. Oper. 26 (4), 388–400. https://doi.org/10.2118/142479-PA.
Singh, K., Bijeljic, B., Blunt, M.J., 2016. Imaging of oil layers, curvature and contact angle in a mixed-wet and a water-wet carbonate rock. Water Resour. Res. 52, 1716–1728. https://doi.org/10.1002/2015WR018072.
Tabatabaei, M., Ghalambor, A., Guo, B., 2012. An analytical solution for water coning in vertical wells. SPE Prod. Oper. 27 (2), 195–204. https://doi.org/10.2118/113106-PA.
Wan, Y., Yong, H., 2015. The key factors affecting the deliverability and OGIP of multi-layer gas reservoirs. In: Abu Dhabi International Petroleum Exhibition and Conference, Abu Dhabi, UAE. https://doi.org/10.2118/177647-MS.
Wang, C.W., Jia, C.S., Peng, X.L., Chen, Z.X., Zhu, S.Y., Sun, H.S., Zhang, J., 2019. Effects of wellbore interference on concurrent gas production from multi-layered tight sands: a case study in eastern Ordos Basin, China. J. Pet. Sci. Eng. 179, 707–715. https://doi.org/10.1016/j.petrol.2019.04.110.
Wang, W., Xie, Q., An, S., Bakhshian, S., Kang, Q., Wang, H., Xu, X., Su, Y., Cai, J., Yuan, B., 2023. Pore-scale simulation of multiphase flow and reactive transport processes involved in geologic carbon sequestration. Earth Sci. Rev. 247, 104602.
Wu, M., Feng, X., Johnson-Paben, R.M., Retterer, S.T., Yin, X., Neeves, K.B., 2012. Single- and two-phase flow in microfluidic porous media analogs based on Voronoi tessellation. Lab Chip 12, 253–261. https://doi.org/10.1039/C1LC20838A.
Yang, H., Fu, J., Liu, X., Meng, P., 2012. Accumulation conditions and exploration and development of tight gas in the Upper Paleozoic of the Ordos Basin. Petrol. Explor. Dev. 39 (3), 315–324. https://doi.org/10.1016/S1876-3804(12)60047-0.
Yang, Y.B., Xiao, W.L., Zheng, L.L., Lei, Q.H., Qin, C.Z., He, Y.A., Liu, S.S., Li, M., Li, Y.M., Zhao, J.Z., Chen, M., 2023. Pore throat structure heterogeneity and its effect on gas-phase seepage capacity in tight sandstone reservoirs: a case study from the Triassic Yanchang Formation, Ordos Basin. Petrol. Sci. 20 (5), 2892–2907. https://doi.org/10.1016/j.petsci.2023.03.020.
Yin, X., Shu, J., Li, Y., Wei, G., Lu, J., Wu, P., Ma, T., 2020. Impact of pore structure and clay content on the water-gas relative permeability curve within tight sandstones: a case study from the LS block, eastern Ordos Basin, China. J. Nat. Gas Sci. Eng. 81, 103418. https://doi.org/10.1016/j.jngse.2020.103418.
Yu, H., Li, W., Qin, X., Wang, Z., Wang, A., Wang, D., Feng, Q., Lan, Y., Wang, Y., 2016. Gas and water distribution of ordovician majiagou formation in northwest of Ordos Basin, NW China. Petrol. Explor. Dev. 43 (3), 435–442. https://doi.org/10.1016/S1876-3804(16)30050-7.
Zaini, M.Z., Du, K., Zhu, M., Feng, L.J., Yang, H.H., Wei, L., Liu, Y., 2019. Yanbei-unlocking the tight gas green field development potential through integrated technology application. In: International Petroleum Technology Conference. https://doi.org/10.2523/IPTC-19265-MS.
Zhang, T., Zhang, L., Wang, Y., Qiao, X., Feng, D., Zhao, W., Li, X., 2020. An integrated well-pattern optimization strategy to unlock continental tight gas reservoir in China. Energy 209, 118449. https://doi.org/10.1016/j.energy.2020.118449.
Zhang, T., Javadpour, F., Li, J., Zhao, Y., Zhang, L., Li, X., 2021. Pore-scale perspective of gas/water two-phase flow in shale. SPE J. 26 (2), 828–846. https://doi.org/10.2118/205019-PA.
Zhang, T., Li, X., Li, J., Feng, D., Li, P., Zhang, Z., Chen, Y., Wang, S., 2017. Numerical investigation of the well shut-in and fracture uncertainty on fluid-loss and production performance in gas-shale reservoirs. J. Nat. Gas Sci. Eng. 46, 421–435. https://doi.org/10.1016/j.jngse.2017.08.024.
Zhao, W., Zhang, T., Jia, C., Li, X., Wu, K., He, M., 2020. Numerical simulation on natural gas migration and accumulation in sweet spots of tight reservoir. J. Nat. Gas Sci. 81, 103454. https://doi.org/10.1016/j.jngse.2020.103454.
Zhao, W., Jia, C., Jiang, L., Zhang, T., He, M., Zhang, F., Jiang, Z., Li, X., Wu, K., 2021. Fluid charging and hydrocarbon accumulation in the sweet spot, Ordos Basin, China. J. Pet. Sci. Eng. 200, 108391. https://doi.org/10.1016/j.petrol.2021.108391.
Zhao, Y., Wang, Z., 2019. Effect of interlayer heterogeneity on multi-seam coalbed methane production: a numerical study using a gray lattice Boltzmann model. J. Pet. Sci. Eng. 174, 940–947. https://doi.org/10.1016/j.petrol.2018.12.006.
Zhao, Y., Zhao, L., Wang, Z., Yang, H., 2019. Numerical simulation of multi-seam coalbed methane production using a gray lattice Boltzmann method. J. Pet. Sci. Eng. 175, 587–594. https://doi.org/10.1016/j.petrol.2018.12.046.
Zhong, G., Li, S., Tang, D., Tian, W., Lin, W., Feng, P., 2022. Study on co-production compatibility evaluation method of multilayer tight gas reservoir. J. Nat. Gas Sci. 108, 104840. https://doi.org/10.1016/j.jngse.2022.104840.
Zou, Q.S., He, X.Y., 1997. On pressure and velocity boundary conditions for the lattice Boltzmann BGK model. Phys. Fluids 9, 1591–1598. https://doi.org/10.1063/1.869307.